HHS Public Access

Author manuscript

Mol Imaging Biol. Author manuscript; available in PMC 2017 February 01.

Published in final edited form as:

Mol Imaging Biol. 2017 February ; 19(1): 130–137. doi:10.1007/s11307-016-0994-1.

Quantitative [^{18}F]-FMISO- PET imaging shows reduction of hypoxia following trastuzumab in a murine model of HER2+ breast cancer

Anna G. Sorace[1], **Anum K. Syed**[2], **Stephanie L. Barnes**[2,3], **C. Chad Quarles**[4], **Violeta Sanchez**[5], **Hakmook Kang**[6], and **Thomas E. Yankeelov**[1,2,3]

[1]Internal Medicine, The University of Texas at Austin, Austin, Texas, USA

[2]Biomedical Engineering, The University of Texas at Austin, Austin, Texas, USA

[3]Institute for Computational and Engineering Sciences, The University of Texas at Austin, Austin, Texas, USA

[4]Division of Imaging Research, Barrow Neurological Institute, St. Joseph's Hospital and Medical Center, Phoenix, AZ, USA

[5]Pathology, Vanderbilt University Medical Center, Nashville, Tennessee, USA

[6]Biostatistics, Vanderbilt University Medical Center, Nashville, Tennessee, USA

Abstract

Purpose—Evaluation of [^{18}F]-FMISO-PET imaging as a metric for evaluating early response to trastuzumab therapy with histological validation in a murine model of HER2+ breast cancer.

Procedures—Mice with BT474, HER2+ tumors, were imaged with [^{18}F]-FMISO-PET during trastuzumab therapy. Pimonidazole staining was used to confirm hypoxia from imaging.

Results—[^{18}F]-FMISO-PET indicated significant decreases in hypoxia beginning on day 3 ($P < 0.01$) prior to changes in tumor size. These results were confirmed with pimonidazole staining on day 7 ($P < 0.01$); additionally, there was a significant positive linear correlation between histology and PET imaging (r^2=0.85).

Conclusions—[^{18}F]-FMISO-PET is a clinically relevant modality which provides the opportunity to 1) predict response to HER2+ therapy before changes in tumor size, and 2) identify decreases hypoxia which has the potential to guide subsequent therapy.

Keywords

FMISO; oxygenation; vascular maturation; Herceptin; BT474; pimonidazole; misonidazole

Corresponding Author: Anna Sorace, PhD, Department of Internal Medicine, Dell Medical School, The University of Texas at Austin, C0800, 1912 Speedway, Austin, TX 78712, anna.sorace@austin.utexas.edu, (P): 512-495-5075.

CONFLICT OF INTEREST

The authors declare that they have no conflicts of interest.

INTRODUCTION

Hypoxia is the reduction of oxygen to tissues below physiological levels (i.e., 15 mmHg, 2% O_2 in tumors [1]) and is generally created by an inadequate blood supply [2]. Tumor hypoxia increases metastatic potential in breast cancer and is a strong prognostic factor of disease progression and survival [3]. Additionally, rapid tumor growth can cause increased consumption of oxygen, along with poor formation of vasculature which impedes sufficient oxygen delivery [4-5]. Radiation therapy, targeted therapies, and chemotherapy are all commonly used for the treatment of breast cancer, and hypoxic tumor cells show resistance to each of these treatment modalities. Hypoxic cells within tumor xenografts have been shown to be resistant to cytotoxic agents that target rapidly dividing cells because of a quiescent nature [6-7]. Furthermore, increased expression of downstream hypoxia cellular markers (e.g., hypoxia-inducible factor 1α (HIF1 α and carbonic anhydrase IX (CA-IX)) in breast cancer biopsies is associated with decreased overall survival [8-10]. Therefore, monitoring the spatiotemporal evolution of hypoxic tissue within a tumor, has the potential to predict eventual response as well as guide subsequent therapy

There are over 230,000 new cases of breast cancer in American women each year, with human epidermal growth factor receptor 2 (HER2) overexpression prevalent in 25% of these patients [11]. HER2+ overexpression in breast cancer is associated with increased recurrence, metastasis, and poorer overall prognosis. Trastuzumab, a standard-of-care therapy in HER2+ breast cancer, is a monoclonal antibody that targets and interferes with the HER2/neu receptor to reduce proliferation through cell cycle arrest [12]. Additionally, as a secondary mechanism of action, trastuzumab suppresses angiogenesis by induction of antiangiogenic factors and inhibition of proangiogenic factors. This alteration in tumor vasculature has been shown through increased vascular maturation [13], decreased release of vascular endothelial growth factor (VEGF) [13-14], and a reduction of vessel diameter and leakiness [14]. Importantly, trastuzumab-induced vascular maturation has been shown to improve perfusion and intratumoral delivery of systemic agents [13]. Similarly, improved hemodynamic efficiency has the potential to decrease hypoxia and enhance the effectiveness of these therapies. The ability to sensitize a tumor to current standard-of-care therapies (chemotherapy, radiation therapy) are of great clinical importance in the treatment of cancer, because it provides a pathway for improving drug efficiency without increasing the total dose.

Positron emission tomography (PET) and magnetic resonance imaging (MRI) methods have been developed that can assess vascular, molecular, and cellular changes prior to changes in tumor size [15-16]. However, the specific evaluation of [^{18}F]-fluoromisonidazole (FMISO)-PET as a predictor of treatment response in HER2+ breast cancer has been undeveloped. [^{18}F]-FMISO freely diffuses into cells and under normal oxidative conditions, freely exits. When entering hypoxic cells, FMISO is reduced and retained through accumulation of the 2-nitroimidazole metabolites and irreversible binding to intracellular thiol-rich proteins [17]. The retention of the tracer in hypoxic tissue makes [^{18}F]-FMISO-PET a highly sensitive and specific, noninvasive imaging technique for detection of tumors that exhibit hypoxia [18-19]. Furthermore, the ability to noninvasively measure hypoxia has the potential to play an

important role for evaluating treatment response, as well as guiding radiation and cytotoxic therapy.

In this effort, we evaluate [^{18}F]-FMISO-PET as a metric for assessing response to trastuzumab therapy in a murine model of HER2+ breast cancer with histological validation. Specifically, the goals of this study are to 1) evaluate early response to trastuzumab treatment prior to changes in tumor size, 2) validate these measurements by correlating imaging and histological assessments, and finally, 3) quantify longitudinal alterations in hypoxia following trastuzumab therapy.

MATERIALS AND METHODS

Animal model

All procedures were approved by our institution's animal care and use committee. BT474 HER2+ cells were grown in improved minimal essential medium (IMEM, Invitrogen, Carlsbad, CA) supplemented with 10% FBS, 1% L-glutamine, and 1% insulin. Cells were grown to 80-90% confluency in 5% O_2 and 37°C. Cells were counted *via* hemocytometer and trypan blue dye exclusion. Nude athymic female mice (N = 37) were subcutaneously implanted with a 0.72 mg, 60-day release, 17β-estradiol pellet (Innovative Research of America, Sarasota, FL) in the nape of the neck. Approximately 24 hours later, 10^7 BT474 breast cancer cells in serum-free IMEM media with 20% growth factor-reduced Matrigel were injected subcutaneously into the right flank of the mouse (cells/100 μl). Tumors were monitored through caliper measurements weekly (ellipsoid tumor volume = (4/3)*π*(length/2)*(width/2)*(height/2)) and, after five weeks of growth, mice were randomly separated into groups (prior to initiation of imaging studies). Animals were treated with either trastuzumab (10 mg/kg) or saline *via* intraperitoneal (i.p.) injection in 100 μl total on day 0 (five weeks post implant, tumor volume = 217.84 ± 32.11 mm^3), immediately following baseline imaging, and day 3, immediately following imaging.

Radiotracer synthesis

[^{18}F]-FMISO was prepared as a service by Vanderbilt University's radiochemistry core. [^{18}F]-FMISO was obtained with average radiochemical purity of 99.82% and specific activity was approximately 33785 Ci/mmol (1.25e15 Bq/mmol).

[^{18}F]-FMISO-PET imaging and analysis

Animals (N = 10; N = 5 treated with trastuzumab, N = 5 treated with vehicle) were imaged with [^{18}F]-FMISO-PET on baseline (day 0), day 1, day 3, day 4 and day 7 (see Fig. 1). At each imaging time point, mice were injected with approximately 350 μCi of [^{18}F]-FMISO (348.80 ± 29.10 μCi (12.9 ± 1.1 MBq), mean ± standard deviation) *via* retro orbital injection and then 70 minutes later were transferred under anesthesia to a Siemens Inveon microPET/CT (Siemens Preclinical Solutions; Knoxville, TN) for rodent imaging to quantify volumetric uptake of [^{18}F]-FMISO. Anesthesia was maintained at a rate of 1.5 % isoflurane in air. Animal body temperature was maintained at 37° C by a heated circulating water pad. Anesthesia was continued, and immediately prior to PET imaging, a high resolution computed tomography (CT) scan was obtained for anatomical localization. CT

was acquired with an x-ray voltage of 80 kVp and a beam intensity of 25 mAs. The CT images were reconstructed into 367 × 367 × 512 voxels at a spatial resolution of 0.114 × 0.114 × 0.114 mm^3. At 80 min post injection, list-mode data were collected for 20 minutes. Images collected for 20 minutes were reconstructed into transaxial slices (128 × 128 × 95) with voxel sizes of 0.95 × 0.95 × 0.8 mm^3, after applying scatter and attenuation corrections using an iterative ordered subsets expectation maximization (OS-EM 2D) algorithm. For accurate measures of injected dose, the needle containing the tracer dose was measured prior to injection and the residual in the needle post injection was also measured.

Parametric maps of the standardized uptake value (SUV) were calculated by normalizing the average activity concentration to animal weight and injected dose. MATLAB was used to manually draw three-dimensional (3D) regions of interest (ROIs) around the entire tumor volume on the SUV maps. CT images were used to confirm tumor location, but did not provide the necessary contrast between tumor and muscle on the ventral side of the tumor to delineate the differences, while PET did. ROIs were also drawn across three slices within the contralateral muscle to serve as controls and the average and max muscle SUV were calculated. Three investigators, who were blinded to treatment groups, defined all ROIs for each mouse at each imaging time point. To eliminate the inconsistencies found with identifying the slices where the tumor begins and ends due to partial voluming tissue with air, the five central slices were utilized to calculate the average, max and hotspot SUVs. Hotspot SUV utilizes the general criteria established in PERCIST [20], and identifies the nine voxels that compose a cube (evaluated through all three planes) whose average SUV in the maximum within the tumor ROI. The average of the results from the three sets of tumor ROIs was used to determine the SUV values for each mouse on each day throughout the study. Hotspot analysis was not completed on the muscle ROI due to the small section used. Inter-user error was calculated by quantifying the standard error between the SUVs calculated from the different ROIs for one tumor. The hotspot SUV from the tumor ROI was selected for statistical comparisons to eliminate potential bias due to tumor necrosis, which would lead to an increase in heterogeneity of radiotracer uptake throughout the whole tumor volume. The one central slice of imaging data was used to further directly compare with histology central slice information.

Immunohistochemistry

Immediately following [^{18}F]-FMISO-PET imaging at day 7, animals were injected with pimonidazole *via* the tail vein. One hour following pimonidazole injection (Hypoxyprobe, Burlington, MA), animals were sacrificed and tumors were cut in half at the largest cross section of the tumor (to allow slices to be obtained from the center of the tumor) and immediately fixed in 10% formalin for 48 hours. Samples were then transferred to 70% ethanol for 72 hours and then processed and embedded in paraffin, and cut into 4 μm sections, floated onto charged glass slides, and dried overnight. For each tumor, one section was stained for hematoxylin and eosin (H&E). Additionally, following antigen retrieval on the remaining sections, the tissue sections were stained with anti-CD31 (DAKO, Carpinteria, CA, Catalog # m7240, antigen retrieval: Citrate Buffer pH 6 (Decloaking Chamber), dilution 1:150, overnight incubation, Envision, DAB (Dako) or anti-pimonidazole (Hypoxyprobe, Burlington, MA, dilution 1:400, overnight incubation, Envision, DAB (Dako)). Slides were

digitally scanned in high resolution (20×) brightfield with a Leica (Leica Microsystems Inc, Ariol, Buffalo Grove, IL) SCN400 Slide Scanner. H&E sections were examined for cellular necrosis and reported as a percentage of tumor cross-sectional area. The software associated with the Leica SCN400 package provided unbiased, semi-automated image analysis and quantification of immunostaining in brightfield. The program was manually trained to identify hypoxia, microvessels, necrosis, and cellularity based on coloring and size thresholding on known positive samples of the histology stain and then automated to be systematically applied to the entire tumor ROI for each histology slice for quantification. Percent hypoxia (i.e., pimonidazole staining) was calculated as the percentage of hypoxic region (as designated by color thresholding) stained in the central slice of the tumor. Pimonidazole immunohistochemistry has been shown to be the gold standard for evaluation of hypoxia to compare to [^{18}F]-FMISO uptake [21-22]. Microvessel density (MVD) was examined through analysis of total microvessels per area (calculated by combination color thresholding and size inclusion) through CD31 staining. Cellular density was calculated as the total number of nuclei per square millimeter for the entire central slice. Percent necrosis (H&E staining) was calculated as the percentage of necrosis (as designated by color thresholding) stained in the central slice of the tumor. Two central slice tumor sections were analyzed and averaged for each histological parameter for comparison with the *in vivo* data on day 7.

Immunofluorescence

Another cohort of animals ($N = 27$) was separated into two groups (treated with trastuzumab and those receiving vehicle) to assess longitudinal changes in hypoxia (pimonidazole) through immunofluorescence. Agent (Hypoxyprobe, Burlington, MA) was injected 1 hour prior to sacrifice between days baseline (zero) through seven. Mice were sacrificed and tumors resected on days zero, one, three, four, and seven for immunofluorescence; there were three treated and three control animals for each time point, except for day zero, in which there were four animals total. Tumors were cut in half at the largest cross-section and were immediately frozen for processing. One central slice per tumor was stained. The tissue sections were stained according to modified manufacturer's protocols with anti-pimonidazole (Hypoxyprobe) with propidium iodide as a nuclear counterstain. Slides were digitally scanned in high resolution (20× magnification). Central slice tumor sections were analyzed for quantification of immunostaining as percent hypoxia.

Statistics

Statistical analysis was completed with GraphPad Prism 6 (GraphPad Software Inc, La Jolla, CA) and R (The R Foundation). Longitudinal [^{18}F]-FMISO-PET and tumor growth parameters were compared within and between cohorts at each time point using the nonparametric Wilcoxon rank sum test. The Friedman test adjusting for multiple comparisons with Dunns was utilized to assess longitudinal changes. The longitudinal changes within and between cohorts were also assessed by fitting mixed-effects linear models while taking into account the underlying temporal correlation. In each model, SUV serves as dependent variable and time and time^2 serve as explanatory variables. The significance of time and time^2 variables in the model assessing the within-cohort change was evaluated. To assess between-cohort change, we added an interaction term between time and

cohort indicator variable in which the statistical significance of the interaction term would be indicative of between-cohort change in SUV. Receiver operating characteristic (ROC) analysis was performed on absolute parameter values on baseline and days one, three, four, and seven to determine the sensitivity of the SUV to separate groups. Histological data was compared using a nonparametric Wilcoxon rank sum test. Linear regression parameters and Pearson correlation coefficients were determined for the central slice analysis for comparisons between percent hypoxia (determined by pimonidazole staining) and SUV (as determined by hotspot analysis of [^{18}F]-FMISO-PET imaging). All data are presented as mean ± standard error (SE) with $P \leq 0.05$ considered significant.

RESULTS

Tumor volume

Changes in tumor volume are displayed for each cohort in Fig 2c. A significant difference in the percent change in tumor volume was observed between the groups at day 7 (P = 0.02). No significant differences were observed on days zero through four (P > 0.05).

[^{18}F]-FMISO-PET Imaging

Representative images of SUV were constructed and tumors are designated by dashed circle in Fig 2a. One representative animal from each cohort is displayed in each of two columns, while the five rows represent the different imaging time points. The mean SUV, SUV hotspot, and SUV max values for each imaging time point are included in Table 1. Additionally the mean SUV and the max SUV values for the muscle are seen in Table 2. The SUV hotspot of the treated cohort was significantly lower on day 3 (P = 0.008), day 4 (P = 0.008), and day 7 (P = 0.008), compared to controls (as seen in Fig 2b), revealing an early response detected by imaging prior to changes in tumor size. There were no significant differences in the SUV hotspot between the control and treated groups at baseline or day 1 (P = 0.15). Additionally, there were no changes seen between the treated and control groups in the muscle ROIs for either the SUV mean or max values at each day (P > 0.05). The Friedman test adjusting for all multiple comparisons evaluating longitudinal changes within each group revealed significant comparisons in the control group (P = 0.003) beginning at day four and trended towards significance in the treated group (P = 0.08). However, mixed-effects models revealed significant change in SUV over time in both the control group (P < 0.001) and the treatment group (P = 0.014), and also disclosed the longitudinal changes in SUV were significantly different between the two groups (P < 0.001).

On day one, the area under the ROC curve was 0.84 (P = 0.08) and 0.54 (P = 0.84), for SUV hotspot and tumor volume, respectively. On day three, ROC analysis showed an area under the curve value of 1.00 (P = 0.009) and 0.70 (P = 0.30), for SUV hotspot and tumor volume, respectively. On day four, ROC analysis of area under the curve value was 1.00 (P = 0.009) and 0.62 (P = 0.53), for SUV hotspot and tumor volume, respectively. On day seven ROC analysis revealed an area under the curve value of 1.00 (P = 0.009) and 1.00 (P = 0.01), for SUV hotspot and tumor volume, respectively.

Histology

Immunohistochemical staining for pimonidazole exhibited a significant decrease in the treated group compared to controls on day seven (P = 0.008), as seen in Fig 3a, b. SUV of central slice analysis also showed a significant difference between treated and controls which was consistent with the tumor volume analysis (P = 0.008), Fig 3c. Furthermore, the percentage of hypoxia for viable tissue per group is significantly different (P < 0.0001) between treated (1.97±1.34) and control (22.97 ± 1.31) groups. Additionally, the comparison of one central slice of the imaging and histology data on day seven showed a significant positive linear correlation (r^2 = 0.85, P < 0.0001), as seen in Fig 3d. Error in SUV is associated with inter-user error, while error in the x-direction is from the averaging different histology slices. Immunohistochemical staining for microvessel density revealed a non-significant increase in the treated group compared to controls on day seven (P = 0.22), as seen in Fig 4a-c. Additionally, evaluations of cellularity showed no significant changes between the groups (P = 0.22) (Fig 4d-f); as well as no significant changes in percent necrosis (P =0.53), as seen in Fig 4g-i.

Longitudinal assessment of histology hypoxia markers

Longitudinal assessment of changes in hypoxia in a separate cohort of mice through immunofluorescence staining revealed (non-significantly) decreased pimonidazole staining in treated tumors compared to controls on day four, with a 28% decrease (P = 0.23), as seen in Fig 5. Immunofluorescence staining for pimonidazole exhibited a significant 45% decrease in the treated group compared to controls on day seven (P = 0.0001, Fig 5).

DISCUSSION

Hypoxia is a prognostic factor of cancer resistance, and reduction of hypoxia has the potential to be an early measure of response to treatment. This study demonstrated that trastuzumab reduces hypoxia in a preclinical model of HER2+ breast cancer. Furthermore, this study evaluated quantitative PET imaging of hypoxia as a predictive imaging metric of response to trastuzumab, separating responders (treated) vs. nonresponders (control group, saline treated) four days prior to significant changes in tumor size. This study also confirmed correlation between [^{18}F]-FMISO-PET imaging and quantitative analysis of pimonidazole (hypoxia) *via* histology in this model. Finally, this study revealed preliminary results evaluating the temporal changes in hypoxia following trastuzumab therapy.

[^{18}F]-FMISO-PET has been shown to be reproducible in a xenograft model of breast cancer [23], further supporting this technique to be utilized as a metric for predicting response to treatment. Other preclinical models have also employed [^{18}F]-FMISO-PET to assess treatment response and have demonstrated that it can be utilized to monitor changes in hypoxia in response to treatment in murine models of colorectal cancer (treatment with DMXAA [24]) and lung cancer (treatment with EGFR targeted therapy [25]). One other preclinical model of HER2+ breast cancer using the mouse mammary tumor virus (MMTV)-polyoma virus middle T (PyMT) derived mammary carcinoma exhibited a significantly decreased SUV in response to sunitinib [26]; though, this study did not evaluate [^{18}F]-FMISO as a predictive metric to evaluate response, but as a secondary method for evaluating

response simultaneously with changes in tumor volume. Additionally, other PET imaging tracers have been evaluated as predictive biomarkers of response to trastuzumab in mouse models [27-28]. To the author's knowledge, the current effort is the first assessment of using [^{18}F]-FMISO-PET to evaluate and predict the response of a HER2+ breast cancer model to trastuzumab.

Limitations of this study include a lack of corresponding histology and imaging data for each time point investigated, which is not possible with a longitudinal imaging study. In particular, the apparent difference in sensitivity between FMISO and pimonidazole between the longitudinal studies likely reflects differences in animal number at each time point, with fewer animals analyzed by histology (n = 3/group/time point) than imaging (n = 5/group/time point). Additionally, multiparametric analysis of vascular delivery (*via* dynamic contrast enhanced MRI [29-30] or contrast enhanced ultrasound [31-32]) could potentially be informative to simultaneously evaluate the correlations and longitudinal effects of oxygenation (hypoxia) and vascularity. Another limitation of this study is the low uptake of [^{18}F]-FMISO compared to normal tissue, though we do note that the SUV values reported for other xenograft models range from 0.06 to 1.2 [24-25], which is consistent with our study. Additionally, trastuzumab reducing hypoxia is in agreement with previously published data on HER2-overexpressing MCF7 cells in a murine model [33]. Despite the limitations, while hypoxia generally increases with tumor size[34] (as seen in the control group), this study reveals that trastuzumab decreases hypoxia prior to changes in tumor size. It is also important to note that there are significant differences between the max SUV values found in the muscle and tumor data (Table 1 and Table 2) indicating that the tumor is a hypoxic environment at the initiation of the study (prior to treatment). Furthermore, previous investigations revealed that trastuzumab improves vascular perfusion into the tumor, therefore, the decreased changes in [^{18}F]-FMISO uptake in the treated group were not simply due to decreased perfusion or delivery of the tracer. Additionally, the imaging time frame at 90 minutes post injection would occur downstream after any initial differences in perfusion or delivery of the contrast agent.

Toxicity is the rate limiting factor for treatment of cancer with cytotoxic therapy. There has been an ongoing efforts to improve patient care through reduction of toxicity and the side effects associated with cancer treatment [35]. Our results provide multiple lines of evidence that trastuzumab reduces hypoxia in BT474, HER2+ breast cancer, tumors. The observed increase in tumor oxygenation (through reduction in hypoxia) initiated by treatment with trastuzumab has the potential to enhance the effectiveness of cytotoxic radiation therapy, without increasing dose or toxic side effects. Previous research has shown that trastuzumab increases the vascular delivery of a secondary agent during this same timeframe [13]. Increasing vascular delivery and reducing hypoxia presents an opportunity to decrease metastatic potential of the tumor, while improving the treatment efficiency. The reduction of cytotoxic side effects and improvement of therapeutic effectiveness has the capability to improve a breast cancer patient's overall health and quality of life. The ability to identify this temporal window via a clinically relevant imaging modality (i.e., [^{18}F]-FMISO-PET) would provide the translational opportunity to optimize therapy on a patient-specific basis.

CONCLUSIONS

Hypoxia is a prognostic factor of cancer resistance, and alleviation of hypoxia has potential to be a marker of response to treatment. This study revealed that trastuzumab significantly reduces hypoxia in a HER2+ breast cancer, providing the opportunity for decreased metastatic potential and increased susceptibility to respond to treatment. Significant changes in hypoxia measured *via* noninvasive imaging were detected four days prior to changes in tumor size, providing an early predictor of response to treatment. This response was confirmed *via* immunohistochemistry. Additionally, positive correlations between histology and imaging of hypoxia in this HER2+ breast cancer model were established. Utilizing a clinically relevant imaging modality provides the opportunity to translate this technique to the clinic for predicting response to therapy, with future potential to guide combination therapies of targeted HER2+ therapy plus cytotoxic treatments, radiation, or chemotherapy.

ACKOWLEDGMENTS

We thank the National Cancer Institute for support through U01CA174706, R01CA138599, R01 CA158079, U01CA142565, and 5T32CA093240. T.E.Y. is a CPRIT Scholar and the W.A. “Tex” Moncrief Professor of Computational Oncology at The University of Texas at Austin. We would like to thank Drs. Michael Freeman and Melinda Sanders for their help with this project.

REFERENCES

1. Hammond EM, Asselin MC, Forster D, O'Connor JP, Senra JM, Williams KJ. The meaning, measurement and modification of hypoxia in the laboratory and the clinic. Clin Oncol (R Coll Radiol). 2014; 26:277–288. [PubMed: 24602562]
2. Helmlinger G, Yuan F, Dellian M, Jain RK. Interstitial pH and pO2 gradients in solid tumors in vivo: high-resolution measurements reveal a lack of correlation. Nat Med. 1997; 3:177–182. [PubMed: 9018236]
3. Gruber G, Greiner RH, Hlushchuk R, et al. Hypoxia-inducible factor 1 alpha in high-risk breast cancer: an independent prognostic parameter? Breast Cancer Res. 2004; 6:R191–198. [PubMed: 15084243]
4. Goel S, Duda DG, Xu L, et al. Normalization of the vasculature for treatment of cancer and other diseases. Physiol Rev. 2011; 91:1071–1121. [PubMed: 21742796]
5. Mankoff DA, Dunnwald LK, Partridge SC, Specht JM. Blood flow-metabolism mismatch: good for the tumor, bad for the patient. Clin Cancer Res. 2009; 15:5294–5296. [PubMed: 19706819]
6. Hill RP, Stanley JA. The response of hypoxic B16 melanoma cells to in vivo treatment with chemotherapeutic agents. Cancer Res. 1975; 35:1147–1153. [PubMed: 1120304]
7. Teicher BA, Lazo JS, Sartorelli AC. Classification of antineoplastic agents by their selective toxicities toward oxygenated and hypoxic tumor cells. Cancer Res. 1981; 41:73–81. [PubMed: 7448778]
8. Generali D, Berruti A, Brizzi MP, et al. Hypoxia-inducible factor-1alpha expression predicts a poor response to primary chemoendocrine therapy and disease-free survival in primary human breast cancer. Clin Cancer Res. 2006; 12:4562–4568. [PubMed: 16899602]
9. Redig AJ, McAllister SS. Breast cancer as a systemic disease: a view of metastasis. J Intern Med. 2013; 274:113–126. [PubMed: 23844915]
10. Weber DC, Tille JC, Combescure C, et al. The prognostic value of expression of HIF1alpha, EGFR and VEGF-A, in localized prostate cancer for intermediate- and high-risk patients treated with radiation therapy with or without androgen deprivation therapy. Radiat Oncol. 2012; 7:66. [PubMed: 22546016]
11. Society, AC. Cancer Facts & Figures 2016. American Cancer Society; Atlanta: 2016.

12. Boekhout AH, Beijnen JH, Schellens JH. Trastuzumab. Oncologist. 2011; 16:800–810. [PubMed: 21632460]
13. Sorace AG, Quarles CC, Whisenant JG, et al. Trastuzumab improves tumor perfusion and vascular delivery of cytotoxic therapy in a murine model of HER2+ breast cancer: preliminary results. Breast Cancer Res Treat. 2016; 155:273–284. [PubMed: 26791520]
14. Izumi Y, Xu L, di Tomaso E, Fukumura D, Jain RK. Tumour biology: herceptin acts as an anti-angiogenic cocktail. Nature. 2002; 416:279–280.
15. Li X, Abramson RG, Arlinghaus LR, et al. Multiparametric magnetic resonance imaging for predicting pathological response after the first cycle of neoadjuvant chemotherapy in breast cancer. Invest Radiol. 2015; 50:195–204. [PubMed: 25360603]
16. Yankeelov TE, Abramson RG, Quarles CC. Quantitative multimodality imaging in cancer research and therapy. Nat Rev Clin Oncol. 2014; 11:670–680. [PubMed: 25113842]
17. Masaki Y, Shimizu Y, Yoshioka T, et al. The accumulation mechanism of the hypoxia imaging probe "FMISO" by imaging mass spectrometry: possible involvement of low-molecular metabolites. Sci Rep. 2015; 5:16802. [PubMed: 26582591]
18. Muzi M, Peterson LM, O'Sullivan JN, et al. 18F-Fluoromisonidazole Quantification of Hypoxia in Human Cancer Patients Using Image-Derived Blood Surrogate Tissue Reference Regions. J Nucl Med. 2015; 56:1223–1228. [PubMed: 26112020]
19. Rajendran JG, Krohn KA. F-18 fluoromisonidazole for imaging tumor hypoxia: imaging the microenvironment for personalized cancer therapy. Semin Nucl Med. 2015; 45:151–162. [PubMed: 25704387]
20. Wahl RL, Jacene H, Kasamon Y, Lodge MA. From RECIST to PERCIST: Evolving Considerations for PET response criteria in solid tumors. J Nucl Med. 2009; 50(Suppl 1):122S–150S. [PubMed: 19403881]
21. Hatano T, Zhao S, Zhao Y, et al. Biological characteristics of intratumoral [F-18]fluoromisonidazole distribution in a rodent model of glioma. Int J Oncol. 2013; 42:823–830. [PubMed: 23338175]
22. Cho H, Ackerstaff E, Carlin S, et al. Noninvasive multimodality imaging of the tumor microenvironment: registered dynamic magnetic resonance imaging and positron emission tomography studies of a preclinical tumor model of tumor hypoxia. Neoplasia. 2009; 11:247–259. 242, 259. [PubMed: 19242606]
23. Whisenant JG, Peterson TE, Fluckiger JU, Tantawy MN, Ayers GD, Yankeelov TE. Reproducibility of static and dynamic (18)F-FDG, (18)F-FLT, and (18)F-FMISO MicroPET studies in a murine model of HER2+ breast cancer. Mol Imaging Biol. 2013; 15:87–96. [PubMed: 22644988]
24. Oehler C, O'Donoghue JA, Russell J, et al. 18F-fluromisonidazole PET imaging as a biomarker for the response to 5,6-dimethylxanthenone-4-acetic acid in colorectal xenograft tumors. J Nucl Med. 2011; 52:437–444. [PubMed: 21321262]
25. Arvold ND, Heidari P, Kunawudhi A, Sequist LV, Mahmood U. Tumor Hypoxia Response After Targeted Therapy in EGFR-Mutant Non-Small Cell Lung Cancer: Proof of Concept for FMISO-PET. Technol Cancer Res Treat. 2016; 15:234–242. [PubMed: 25759424]
26. Theze B, Bernards N, Beynel A, et al. Monitoring therapeutic efficacy of sunitinib using [(18)F]FDG and [(18)F]FMISO PET in an immunocompetent model of luminal B (HER2-positive)-type mammary carcinoma. BMC Cancer. 2015; 15:534. [PubMed: 26198000]
27. Shah C, Miller TW, Wyatt SK, et al. Imaging biomarkers predict response to anti-HER2 (ErbB2) therapy in preclinical models of breast cancer. Clin Cancer Res. 2009; 15:4712–4721. [PubMed: 19584166]
28. Kramer-Marek G, Gijsen M, Kiesewetter DO, et al. Potential of PET to predict the response to trastuzumab treatment in an ErbB2-positive human xenograft tumor model. J Nucl Med. 2012; 53:629–637. [PubMed: 22410461]
29. Yang X, Knopp MV. Quantifying tumor vascular heterogeneity with dynamic contrast-enhanced magnetic resonance imaging: a review. J Biomed Biotechnol. 2011; 2011:732848. [PubMed: 21541193]

30. Padhani AR. Dynamic contrast-enhanced MRI in clinical oncology: current status and future directions. J Magn Reson Imaging. 2002; 16:407–422. [PubMed: 12353256]
31. Hudson JM, Williams R, Tremblay-Darveau C, et al. Dynamic contrast enhanced ultrasound for therapy monitoring. Eur J Radiol. 2015; 84:1650–1657. [PubMed: 26231046]
32. Balleyguier C, Opolon P, Mathieu MC, et al. New potential and applications of contrast-enhanced ultrasound of the breast: Own investigations and review of the literature. Eur J Radiol. 2009; 69:14–23. [PubMed: 18977102]
33. Hardee ME, Eapen RJ, Rabbani ZN, et al. Her2/neu signaling blockade improves tumor oxygenation in a multifactorial fashion in Her2/neu+ tumors. Cancer Chemother Pharmacol. 2009; 63:219–228. [PubMed: 18365198]
34. Li XF, O'Donoghue JA. Hypoxia in microscopic tumors. Cancer Lett. 2008; 264:172–180. [PubMed: 18384940]
35. Cleeland CS, Allen JD, Roberts SA, et al. Reducing the toxicity of cancer therapy: recognizing needs, taking action. Nat Rev Clin Oncol. 2012; 9:471–478. [PubMed: 22751283]

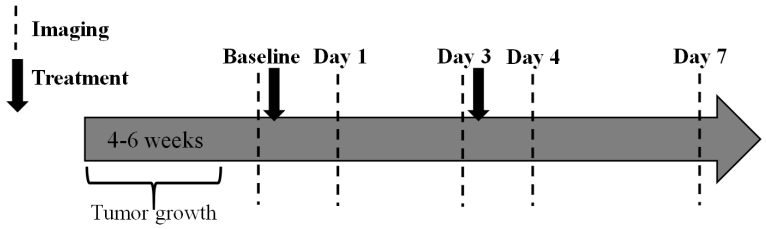

Fig 1.
Outline of tumor implantation, imaging and treatment schedule.

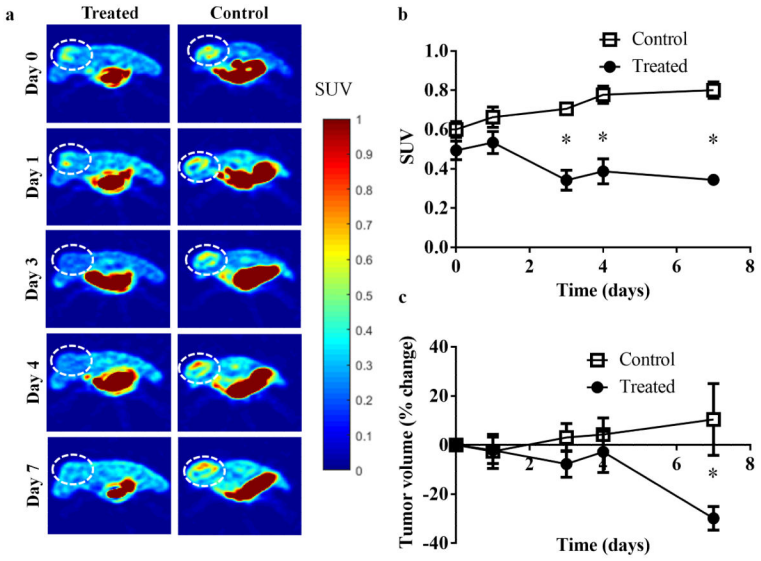

Fig 2.

a Longitudinal [^{18}F]-FMISO-PET central slice images of a representative control and treated animal (tumor denoted by dashed circle) over seven days. [^{18}F]-FMISO retention increased longitudinally in the control mouse, in contrast to the observed decrease in the trastuzumab-treated mouse. **b** Graph revealing group mean of hotspot SUV in control versus treated tumors. [^{18}F]-FMISO uptake in treated tumors is significantly lower than controls as early as day three (P = 0.008). **c** Graph of tumor volume changes in response to treatment over seven days. Day seven reveals a significant difference between the groups (P = 0.02).

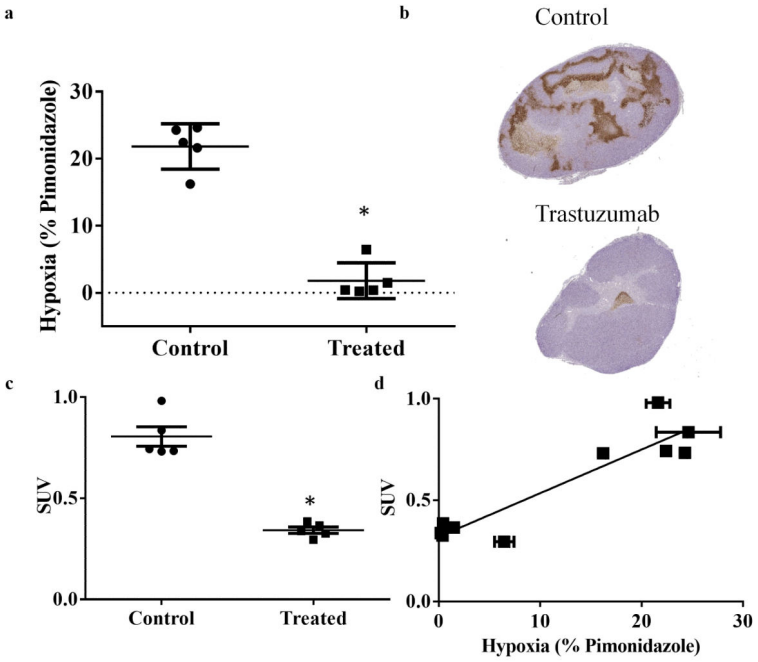

Fig 3.

Correlation of hypoxia imaging and histology is shown through central slice analysis of the treated and control tumors. **a** Graph revealing quantitative analysis of percent hypoxia staining from histology. Treated tumors reveal significantly decreased hypoxia compared to controls. **b** Representative histology central slices showing overall hypoxia (as stained with pimonidazole, brown) in the treated and control animals. **c** Day seven scatterplot of central slice SUV comparing treatment and controls. **d** Quantitative hypoxia imaging (SUV hotspot) and quantitative histology shows a positive linear correlation ($r^2 = 0.85$, $P < 0.001$).

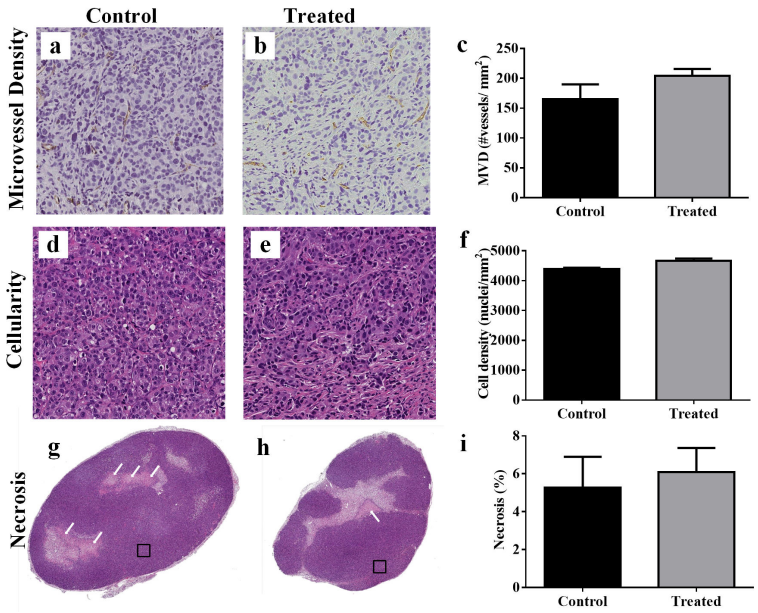

Fig 4.

Quantitative analysis comparing treated and control tumors and representative histology sections are shown for H&E and CD31. CD31 microvessel density (MVD) is shown for **a** control and **b** treated tumors; **c** quantitative analysis reveals no significant changes between the groups on day seven (P = 0.22). H&E cellularity is shown for **d** control and **e** treated tumors; **f** quantitative analysis reveals no significant difference in cellularity in treated tumors compared to controls on day seven (P = 0.22). H&E percent necrosis is shown for **g** control and **h** treated tumors; **i** quantitative analysis reveals no significant changes in necrosis in treated tumors compared to controls on day seven (P = 0.53). Squares in **g** and **h** demonstrate the representative regions displayed in tiles **a**,**c** and **b**,**d**, respectively.

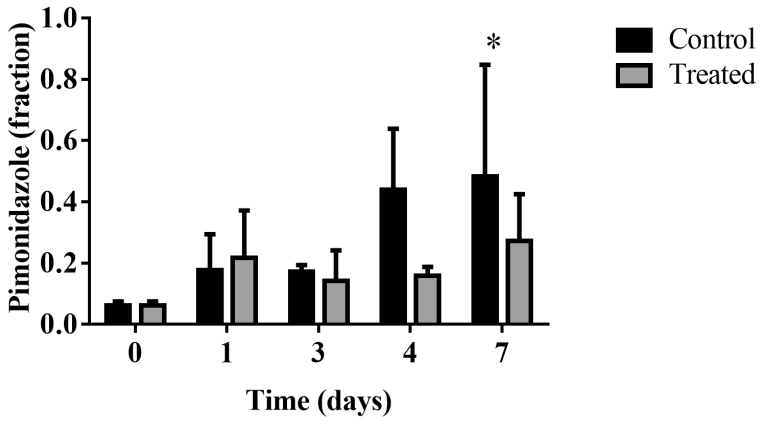

Fig 5.

Longitudinal immunofluorescence analysis of pimonidazole in separate cohorts of mice over 7 days confirm trends of decreased hypoxia markers in trastuzumab-treated tumors.

Table 1

Mean SUV, hotspot SUV and max SUV for tumor *in vivo* longitudinal data

		Day 0	Day 1	Day 3	Day 4	Day 7
Control	*Mean SUV*	0.36 ± 0.03	0.38 ± 0.03	0.37 ± 0.03 *	0.41 ± 0.03 *	0.44 ± 0.03 *
	Hotspot SUV	0.60 ± 0.04	0.66 ± 0.05	0.70± 0.02 *	0.77 ± 0.04 *	0.74 ± 0.09 *
	Max SUV	0.70 ± 0.04	0.75 ± 0.07	0.80± 0.04 *	0.87 ± 0.05 *	0.89 ± 0.05 *
Treated	*Mean SUV*	0.32 ± 0.02	0.32 ± 0.02	0.22 ± 0.03	0.26 ± 0.02	0.26 ± 0.01
	Hotspot SUV	0.49 ± 0.04	0.53 ± 0.05	0.34 ± 0.05	0.39 ± 0.06	0.35 ± 0.05
	Max SUV	0.57 ± 0.06	0.60 ± 0.07	0.42± 0.06	0.44 ± 0.07	0.39 ± 0.02

Table 2

Mean SUV and max SUV for muscle *in vivo* imaging longitudinal data

		Day 0	Day 1	Day 3	Day 4	Day 7
Control	*Mean SUV*	0.28 ± 0.02	0.33 ± 0.02	0.31 ± 0.02	0.33 ± 0.02	0.32 ± 0.02
	Max SUV	0.34 ± 0.03	0.41 ± 0.02	0.37 ± 0.02	0.39 ± 0.02	0.40 ± 0.02
Treated	*Mean SUV*	0.29 ± 0.01	0.33 ± 0.02	0.30 ± 0.02	0.32 ± 0.02	0.30 ± 0.02
	Max SUV	0.36 ± 0.03	0.39 ± 0.02	0.35 ± 0.02	0.37 ± 0.02	0.37 ± 0.02